Kinetic Alfvén Wave Turbulence and Transport through a Reconnection Diffusion Region

C. C. Chaston,[1] J. R. Johnson,[2] M. Wilber,[1] M. Acuna,[3] M. L. Goldstein,[3] and H. Reme[4]
[1]*Space Science Laboratory, University of California, Berkeley, California, USA*
[2]*Princeton Plasma Physics Laboratory, Princeton University, Princeton, USA*
[3]*NASA Goddard Space Flight Center, Greenbelt, Maryland, USA*
[4]*CESR, Toulouse, France*
(Received 8 August 2008; published 8 January 2009)

We demonstrate from observations that kinetic Alfvén waves may play an important role in facilitating magnetic reconnection. These waves radiate outwards from the diffusion region oblique to the magnetic field in a conelike pattern delimited by the X line separatrices with outward energy fluxes equivalent to that contained in the outstreaming ions. It is shown that the wave vectors reverse across the X and symmetry lines and have a large out of plane component. We estimate that these waves drive significant transport through the diffusion region.

DOI: 10.1103/PhysRevLett.102.015001 PACS numbers: 94.30.cp, 52.35.Ra, 94.05.Lk, 94.30.cq

In the presence of a guide magnetic field, the dynamics in reconnection diffusion regions may be described in terms of generalized kinetic Alfvén waves (KAWs) [1,2]. The importance of KAWs in magnetic reconnection may be evaluated from the microphysics of wave-particle interactions in the electric and magnetic fields they carry [3] and macroscopically through consideration of their contribution to the energetics or the effective radiation resistance [4,5] that their emission represents. In this Letter, we exploit multipoint observations from the Cluster spacecraft [6] through a reconnection diffusion region to identify KAW wave-vector morphology and evaluate the importance of these waves in the reconnection process.

Figure 1 shows observations from the Cluster spacecraft while crossing the Earth's neutral sheet at a distance of ~18 Earth radii antisunward of the Earth. This interval was identified by Ref. [7] as a transition through a reconnection ion diffusion region. The 4 Cluster spacecraft at this time were separated by ~150 km. Figure 1(a) shows the trajectory of the spacecraft through the X line. This trajectory represents the motion of the center of the Cluster tetrahedron in the frame of the magnetic field structure (or current sheet) [Fig. 1(b)] determined from the measurement of the plasma flows [Fig. 1(c)], a cross-correlation analysis of the slowly varying (>100 s) magnetic field between spacecraft [U_{ZGSM}, Fig. 1(d); GSM denotes geocentric solar magnetospheric coordinates] and estimates of the current from application of the "curlometer" technique [Fig. 1(e)]. We find that the minimum and maximum variance directions derived both from the curlometer current and from the magnetic field measured from each spacecraft are primarily in the Z_{GSM} and X_{GSM} directions, respectively, with some variation as the spacecraft traverses the symmetry line. These directions are consistent with that obtained from the interspacecraft cross-correlation analysis. Consequently, the X, Y, and Z GSM directions correspond to the usual reconnection L, M, and N coordinates. We also find a guide field averaged over this interval of ~5 nT.

In GSM coordinates, Figs. 1(b)–1(e) indicate that the magnetic field structure moved initially upward (+Z) taking the spacecraft from a region of strong field strength and no flow at 23:28 UT into one of weaker fluctuating fields after 23:28:30 UT with tailward ion flow. We observe intensification in J_y and J_x beginning at 23:28:20 and a reversal in J_x at 23:28:30 consistent with the reversal of the nearly field-aligned currents which close Hall currents across reconnection separatrices. A second reversal in J_x is observed at 23:29:40 UT coincident with a reversal in the ion flow direction shown in Fig. 1(c). Subsequently, the spacecraft enter a region of further intensified J_Y and pass through a point of low magnetic field strength at 23:30:30 UT. This point corresponds to the spacecraft passage through the symmetry line. Integrating U_{ZGSM} in time from 23:28:30 UT until the symmetry line crossing

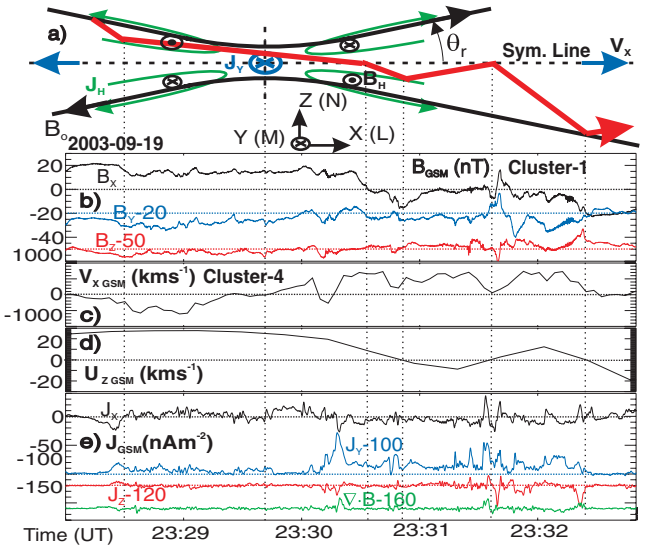

FIG. 1 (color). (a) X line crossing schematic in GSM. (b) Magnetic field. (c) Ion flow along X_{GSM}. (d) Current sheet motion in Z_{GSM}. (e) $\nabla \times B/\mu_o$ and $\nabla \cdot B/\mu_o$.

yields a distance in Z of $\sim 1400 \pm 1000$ km with the uncertainty due to variation with alternate correlation lengths. The current sheet motion after the symmetry line crossing becomes oscillatory in $U_{Z\,\mathrm{GSM}}$.

The normalized reconnection rate can be approximated as $M_o \approx \tan\theta_r = B_z/B_x$, where θ_r is the half-angle of the outflow region identified in Fig. 1(a). The value of B_z/B_x averaged over the four spacecraft through the current sheet is $M_o \approx 0.16$ and is consistent with previous rates observed for reconnection in the Earth's magnetosphere [8]. The reconnection rate may also be defined as $M_o \approx 2d/L$, where d is the half width of the diffusion region in the Z direction and L is its length along X. d may be estimated from Ampere's law as $J_y \approx B_{\mathrm{ox}}/(\mu_o d)$, where $B_{\mathrm{ox}} = 17$ nT is the magnetic field along X on the outer edge of the current sheet. J_y has already been determined from the curlometer technique shown in Fig. 1(e) and has an average value of $J_{y\_\mathrm{av}} = 1.8 \times 10^{-8}$ A/m^2. This yields $d \approx 730$ km, which is within the range defined by the cross-correlation analysis, and provides $L \approx 9140$ km. The average density observed over the interval shown in Fig. 1 is ~ 0.1 cm^{-3}, which yields an ion inertial length of 710 km. M_o can equivalently be defined as v_z/v_x, where v_z is the inflow speed and v_x the outflow speed. The inflow speed is difficult to measure; however, the outflow speed, averaged over the interval shown in Fig. 1(c), is $v_x \sim 300$ km/s and so $v_z \sim 48$ km/s. v_z is determined by the transport rate through the diffusion region and can be estimated as $v_z = D/d$, where D is an effective diffusion coefficient averaged over d. To provide $v_z \sim 48$ km/s requires $D \sim 3.5 \times 10^{10}$ m^2/s. D provides a metric enabling us to evaluate the importance of the integrated effects of wave action through the diffusion region or over that region where demagnetization takes place. Interestingly, for the average plasma parameters observed ($B_o = 14.5$ nT; $n_o = 0.1$ cm^{-3}; $T_i = 5670$ eV, $T_e = 1580$ eV), D is approximately the Bohm diffusion coefficient.

Figure 2(a) shows the transverse magnetic (B_{XFAC}) and electric field (E_{YFAC}) fluctuations observed on Cluster 2 in field-aligned coordinates (FAC). Y_{FAC} lies in the spacecraft spin plane orthogonal to the projection of $\mathbf{B}_o$ into this plane, and Z_{FAC} is field-aligned. This coordinate system is chosen to provide a component of $\mathbf{E}$ perpendicular ($\perp$) to $\mathbf{B}_o$ from spin plane measurements without assuming $\mathbf{E} \cdot \mathbf{B}_o = 0$ for the purpose of dispersion analyses. The spectrograms of B_{XFAC} and E_{YFAC} are shown in Figs. 2(b) and 2(c) and reveal no structuring at either the H^+ gyro frequency (f_p) or the lower hybrid frequency (f_{LH}). Comparison with Figs. 2(d) and 2(e) shows that enhanced spectral energy densities are correlated with fluxes of field-aligned electrons suggesting wave heating/acceleration in parallel to B_o wave electric fields ($E_\parallel$). Based on mode identification, we will show momentarily that, while $E_\parallel$ for these waves is finite, $E_\parallel/E_\perp \ll 1$. This allows us to use $E \cdot B_o \approx 0$ to estimate the outflowing Poynting flux (S_X in GSM) shown in Fig. 2(f). For instrumental reasons, this calculation is also subject to the condition that B_o be $>6°$ from the spin plane which leads to small gaps in S_X.

Comparison of S_X with the energy flux (ε_X) of the ion jets [red line in Fig. 2(f)] reveals that they generally share the same orientation. Averaging ε_X and S_X along the spacecraft trajectory, we find $S_{\mathrm{av}}/\varepsilon_{\mathrm{av}} \approx 0.9$, where S_{av} and $\varepsilon_{\mathrm{av}}$ are the total of the average energy flux in $\pm X_{\mathrm{GSM}}$ directed outflow jets. Hence the fluctuating fields are an important sink for magnetic field energy liberated by reconnection. This result can be checked for energy conservation. The total outflow energy flux is $\xi_{\mathrm{outflow}} \approx 2(v_x B_{\mathrm{out}}{}^2/2\mu_o) +$

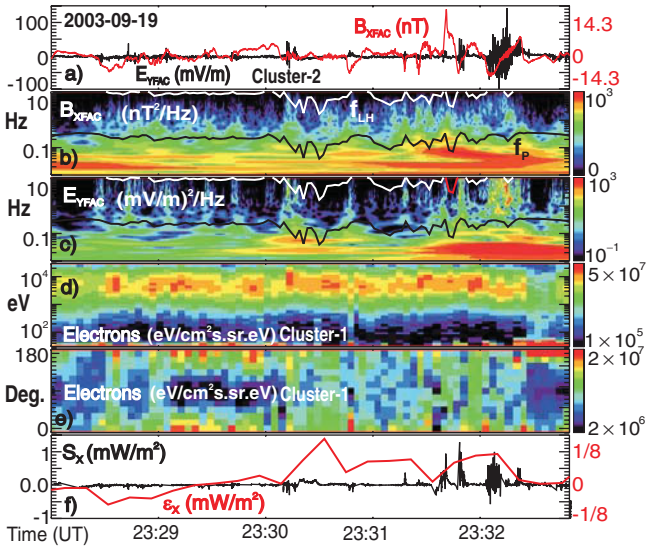

FIG. 2 (color). (a) B_{XFAC} and E_{YFAC} as defined in text. (b) B_{XFAC} dynamic spectrogram; the white line is the lower hybrid frequency (f_{LH}), and the black line the H^+ gyro frequency (f_p). (c) E_{YFAC} dynamic spectrogram. (d) e^- energy spectrogram. (e) e^- pitch angle spectrogram. (f) Poynting flux (S_X) and ion energy flux (ε_X) along X_{GSM}.

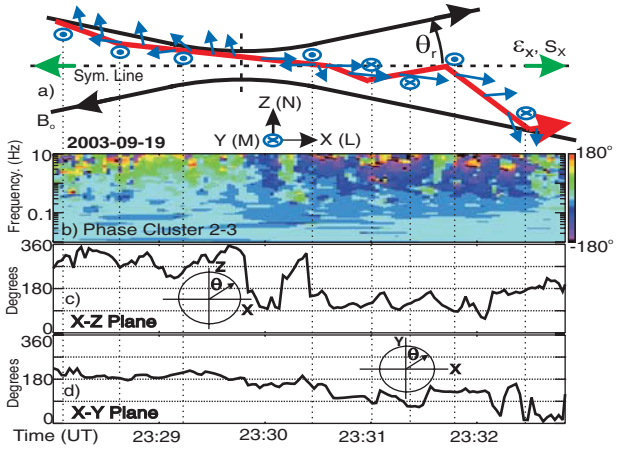

FIG. 3 (color). (a) k orientation schematic. (b) Phase in B between spacecraft 2 and 3. (c),(d) Orientation of k in X-Z_{GSM} and X-Y_{GSM} planes.

$S_{av} + \varepsilon_{av} \approx 1.5 \times 10^{-4}$ W/m^2 and is dominated by the S_{av} and ε_{av} contributions. The inflow energy flux is $\xi_{inflow} \approx 2(v_z B_{in}^2/2\mu_o) \approx 2.4 \times 10^{-5}$, where $B_{in} \approx 25$ nT is defined in the inflow region outside the separatrices, and the small inflow wave and particle energy flux contributions have been ignored. Hence $\xi_{inflow} \approx \xi_{outflow} M_o$ as required for energy conservation.

Figure 3(a) provides a schematic of the k orientation based on the results shown in Figs. 3(b)–3(d) derived from interferometry [9]. In Fig. 3(b), we show the relative phase between spacecraft 2 and 3 which are separated largely along the X direction. Over this interval a phase reversal occurs as the spacecraft traverse the flow reversal with 2 leading 3 before 23:29:40 and 3 leading 2 afterwards. Hence, the phase fronts move outward from the reconnection X line. Figures 3(c) and 3(d) show the orientation of k derived using all four spacecraft over bandwidth in the spacecraft frame from 0.01–1 Hz where $\theta_{xz} = \tan^{-1}(k_x/k_z)$ and $\theta_{xy} = \tan^{-1}(k_x/k_y)$. In the $X - Z$ ($X - Y$) plane, 0° and 90° correspond to k aligned with the $+Z(+Y)$ and $+X$ directions, respectively. Before the X line crossing, we find that in the $X - Z$ plane k points primarily in the $+Z$ direction and in the $X - Y$ plane points largely in the $-Y$ direction. In both planes at this time k is canted in the direction of outward ($-X$) ion flow. After traversing the flow reversal at 23:29:30 UT, the spacecraft remained close to the symmetry line and in the $X - Z$ plane k points in the X direction (i.e., $\theta_{xz} \sim 90°$) close to the direction of the flow. As the spacecraft moves in $-Z$ away from the symmetry line k tends toward the $-Z$ and $+Y$ directions and again remains canted in the flow direction particularly in the $X - Z$ plane. We note that $|k|$ in each plane is comparable. Consequently, k reverses in the out of plane (or Y) direction across the symmetry line and transitions from 0°–90° in the $X - Z$ plane with respect to the symmetry line with motion towards the separatrices. Together with the outward radiating S_X, these observations show that wave emission from the X line has some similarity to that from a localized source in laboratory plasmas [10,11].

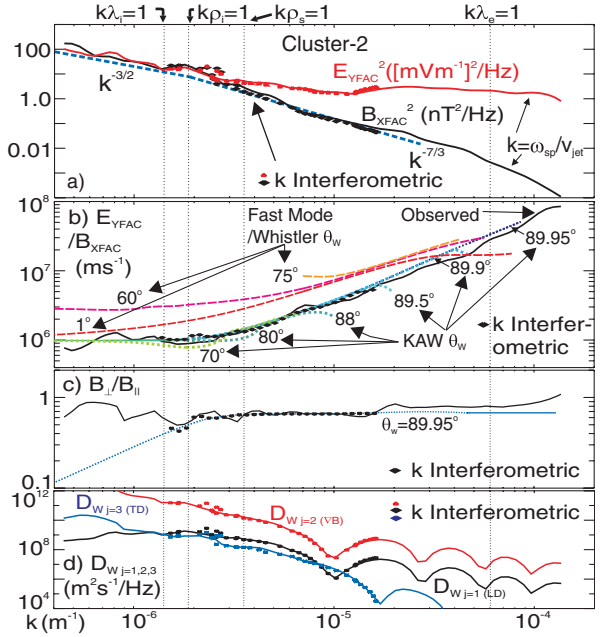

FIG. 4 (color). (a) $B_{YFAC}{}^2$ and $E_{YFAC}{}^2$ spectrograms from interferometry (symbols) and Doppler shift. (b) E_{YFAC}/B_{YFAC} observed and predicted results for KAWs and whistlers. (c) $B_\perp/B_\parallel$ observed and predicted result for KAWs at $\theta_W = 89.95°$. (d) D_W spectrogram as described in text. λ_i and λ_e denote the ion and electron inertial lengths, respectively. ρ_i and ρ_s denote the ion and ion acoustic gyroradii.

Figure 4(a) shows the k spectra of the observed field fluctuations averaged over the interval shown in Fig. 1. In deriving these quantities we have performed the rotation to FAC in ω_{sp} space and determined k from interferometry (symbols) and the approximation $k \approx \omega_{sp}/v_{jet}$, where ω_{sp} and v_{jet} are the frequency and ion flow speed, respectively, in the spacecraft frame. We find approximate agreement between the results from both techniques suggesting that the wave phase speed in the ion frame along the flow direction is much less than the ion flow speed. This eliminates whistlers and lower hybrid waves as candidate wave modes since for these modes $\omega/k > V_A > v_{jet}$ (V_A denotes Alfvén speed). In B_x we can identify power law variations with $k^{-3/2}$ for $k\rho_i \leq 1$ and $k^{-7/3}$ for $k\rho_i > 1$ (ρ_i denotes ion gyroradii). A similar trend is found in E_y for $k\rho_i \leq 1$ with a gentler slope for $k\rho_i > 1$ to provide an increasingly electrostatic wave with increasing k. Interferometry yields $k_\perp/k_\parallel \geq 2 \rightarrow 4$ as $k\rho_i = 1 \rightarrow 8$, where the inequality arises because scales along B_o ($\lambda_\parallel$) provide phase differences at the limit of our resolution.

Figure 4(b) shows the observed E_{YFAC}/B_{XFAC} ratio and that expected for KAW and fast mode/whistler waves from the full hot plasma dispersion tensor using the average parameters given above. We find good agreement between the observed ratio and that expected for KAWs with increasing $\theta_W = \arctan(k_\perp/k_\parallel)$ as k increases. The ratio for the whistler mode over this k range provides a poor fit for all θ_W. We note that the correction $E_{YFAC} = E'_{YFAC} + (\mathbf{v} \times B)_{YFAC}$ to bring E_{YFAC} from the spacecraft frame to the plasma frame (E'_{YFAC}) is $\leq 30\%$ in E_{YFAC}/B_{XFAC} and for reconnection flows effectively zero since $\mathbf{v}_x B_z \approx v_z B_x$. A similar analysis is applied to the $B_\perp/B_\parallel$ ratio in Fig. 4(c), which also shows consistency with KAWs for $k\rho_i \geq 1$. As KAWs, these waves provide finite $E_\parallel$ yet satisfy $E_\parallel/E_\perp \ll 1$ as used to estimate S_X in Fig. 2(f).

KAWs radiate from a localized source, such as the ion diffusion region, within a cone of angular extent given by $\theta_c \approx 0.385(\omega/\Omega_i)[(T_i + T_e)/m_i]^{1/2}/V_A$ radians [10,11]. For $\omega(k)$ the largest frequency KAWs will propagate along the edges of the cone yet retain $\omega/\Omega_i < 1$. From observations, the angular range over which these waves are observed is delineated by the extent of the outstreaming ions.

From above, this range is defined as $\theta_r = \arctan(M_o) \approx 9°$. Consequently, the frequency for the temperatures given earlier, which provides $\theta_c = \theta_r$, is $\omega_{\theta c}/\Omega_i = 0.5$ and hence $\omega(k)/\Omega_i \leq 0.5$ consistent with KAW wave frequencies.

Since $V_A \sim v_i$ (denotes ion thermal speed), these waves are subject to ion damping which may lead to cross-field transport. Using a quasilinear treatment of the gyrokinetic equation, we generalized the drift-kinetic diffusion coefficient due to Landau damping (LD) [12] to also include transport resulting from magnetic field gradient drift (∇B) and transit time damping (TD) [3]

$$D_W \approx \left(\frac{\pi}{8}\right)^{1/2} \sum_{j=1}^{6} \sum_{k} \frac{1}{|k_\parallel| v_i} \left(\frac{|E_Y(k)|}{B_o}\right)^2 d_j, \qquad (1)$$

where $n v_{z\_w} = -D_w \nabla_z n$ and v_{z_w} is the velocity of the plasma across the magnetic field. Here $d_1 = \eta^2 {R_{00}}^0$, $d_2 = \alpha^2(1+\eta)^2 {R_{00}}^4$, $d_3 = 2(\sigma^2\eta^2)/({k_\perp}^2\rho_i^2){R_{11}}^2$, $d_4 = -2\alpha\eta(1+\eta){R_{00}}^2$, $d_5 = 2^{3/2}(\sigma\eta^2)/(k_\perp\rho_i){R_{10}}^1$, and $d_6 = -2^{3/2}\sigma\alpha\eta(l+\eta)/(k_\perp\rho_i){R_{10}}^3$. $d1$, $d2$, and $d3$ are the LD, ∇B, and TD terms, respectively, and d_{4-6} are cross terms. There is also a contribution due to curvature drift which we have not included. $\alpha = \omega_d/\omega$, where $\omega_d = \mathbf{k} v_i \cdot [B/|B| \times \rho_i \nabla B/B]$ is the drift frequency, $\eta = -k_\perp E_\parallel / k_\parallel E_\perp$, and $\sigma = E_{\parallel \mathrm{TD}}/E_\parallel$, where $E_{\parallel \mathrm{TD}} \approx -i[m_j v_i^2/(2B_o)]k_\parallel B_\parallel(k)/q_i$ is the effective $E_\parallel$ due to the wave ion mirror force. Also,

$$R^l_{nm} = 2\int_0^\infty dx x^{l+1} J_n(bx) J_m(bx) \exp[-x^2 - (\zeta - \zeta_d x^2)^2], \qquad (2)$$

where $b = \sqrt{2}k_\perp \rho_i$, $\zeta = \omega/(\sqrt{2}k_\parallel \mathbf{v}_i)$, $\zeta_d = \omega_d/(\sqrt{2}k_\parallel \mathbf{v}_i)$, and J are Bessel functions. Equation (1) provides meaningful estimates for D_W for $\lambda_\perp < L_B \approx \lambda_i$, where L_B is the gradient scale of the magnetic field and $\omega_d \sim k_\perp v_i \rho_i / L_B$. However, as indicated above, over this $\lambda_\perp$ range there is significant uncertainty in $\lambda_\parallel$ ($k_\parallel$). Allowable values for $k_\parallel$ must be small enough to provide $\omega/\Omega_i < 1$ for consistency with the E_Y/B_X ratio shown in Fig. 4(b) yet correspond to parallel scales of the order of the ion diffusion region ($L \approx$ 9140 km) in X or less. These criteria restrict $k_\parallel$ to $\sim 1 \times 10^{-7}$ m^{-1}. Substituting this $k_\parallel$ and using $E_{\mathrm{YFAC}}(k)$ and $B_\parallel(k)$ with KAW wave dispersion yields the curves shown in Fig. 4(d), where we plot the contributions from LD, ∇B, and TD. Summing over $k > 2\pi/\lambda_i$ and $j = 1$–6, we find $D_W \sim 10^{10}$ m^2/s similar to D with the ∇B contribution dominant. For density gradients a small fraction of a cm^{-3} across the diffusion region D_W in the plasma frame will provide inflow speeds comparable to v_z.

The importance of KAWs can also be estimated from the dissipation that their emission represents. For a diffusion region of width h across the magnetotail, the total power radiated from the outflow regions is $P_W = \iint S_x dy dz \approx S_{\mathrm{av}} \times 2d \times h$, where $S_{\mathrm{av}} = 6.8 \times 10^{-5}$ W/m^2 is the average magnitude of the radiated S_x we observe over the interval shown in Fig. 2. Since $P_W = {I_y}^2 R$, where $I = \iint J_Y dx dz \approx J_{y\_\mathrm{av}} \times L \times 2d$ is the total current through the diffusion region and R is the resistance, the resistivity due to radiation resistance is $\eta_{\mathrm{rad}} = 4d^2 L S_W / I^2 = S_{\mathrm{av}}/(J y^2 L) = D_{\mathrm{rad}} \mu_o$. Using the averaged values, this yields $D_{\mathrm{rad}} \sim 10^{10}$ m^2/s similar to D. With $M_o = v_z/v_x = 2d/L$ and taking $v_z = D_{\mathrm{rad}}/d$, L can be eliminated, and we find that if radiation resistance due to these waves accounts for the observed transport, then

$$S_{\mathrm{av}}/(\mu_o v_x {J_y}^2 2d^2) \approx 1 \qquad (3)$$

independent of M_o and related to the fraction of magnetic energy converted to EM waves. For the observed averaged values, this ratio is $\sim$0.5.

This analysis shows that KAWs play an important role in magnetic reconnection. We estimate that KAWs are radiated from the X line with energy flux equivalent to that in the outward streaming ions and may drive significant transport. These waves obey spectral trends expected for MHD turbulence on large isotropic scales ($k_\perp/k_\parallel \sim 1$; $k^{-3/2}$) and for KAWs on small anisotropic ($k_\perp/k_\parallel > 1$; $k^{-7/3}$) subgyroradii scales [13]. We show that these waves propagate with phase fronts which expand from the X line in both the X and the Z directions in a manner that may be consistent with the cone structure expected for KAWs radiating from a localized source. k has a large out of plane (Y) component which underscores the 3D nature of the reconnection process observed.

This research was supported by NSF Grant No. ATM-0602728 and NASA Grants No. NNG05GL27G-06/08, No. NNH07AF37I, and No. NNG07EK69I. We appreciate input from F. Mozer, I. Roth, and J. Eastwood.

[1] J. F. Drake, Geophys. Monogr. Ser. **90**, 155 (1995).
[2] B. N. Rogers *et al.*, Phys. Rev. Lett. **87**, 195004 (2001).
[3] J. R. Johnson and C. Z. Cheng, Geophys. Res. Lett. **24**, 1423 (1997).
[4] P. M. Bellan, Phys. Plasmas **5**, 3081 (1998).
[5] Y. Song and R. L. Lysak, Geophys. Monogr. Ser. **118**, 11 (2000).
[6] C. P. Escoubet *et al.*, Space Sci. Rev. **79**, 11 (1997).
[7] A. L. Borg *et al.*, Geophys. Res. Lett. **32**, L19 105 (2005).
[8] F. S. Mozer and A. Retino, J. Geophys. Res. **112**, A10 206 (2007).
[9] C. C. Chaston *et al.*, Phys. Rev. Lett. **95**, 065002 (2005).
[10] G. J. Morales and J. E. Maggs, Phys. Plasmas **4**, 4118 (1997).
[11] N. Singh, Geophys. Res. Lett. **34**, L13 106 (2007).
[12] A. Hasegawa and K. Mima, J. Geophys. Res. **83**, 1117 (1978).
[13] G. G. Howes *et al.*, J. Geophys. Res. **113**, A05103 (2008).